

Quantum theory of the nonlinear Hall effect

Z. Z. Du,^{1,2} C. M. Wang,^{3,1,2} Hai-Peng Sun,^{1,2} Hai-Zhou Lu,^{1,2,*} and X. C. Xie^{4,5,6}

¹*Shenzhen Institute for Quantum Science and Engineering and Department of Physics, Southern University of Science and Technology (SUSTech), Shenzhen 518055, China*

²*Shenzhen Key Laboratory of Quantum Science and Engineering, Shenzhen 518055, China*

³*Department of Physics, Shanghai Normal University, Shanghai 200234, China*

⁴*International Center for Quantum Materials, School of Physics, Peking University, Beijing 100871, China*

⁵*Beijing Academy of Quantum Information Sciences, Beijing 100193, China*

⁶*CAS Center for Excellence in Topological Quantum Computation,*

University of Chinese Academy of Sciences, Beijing 100190, China

(Dated: April 21, 2022)

The nonlinear Hall effect is an unconventional response, in which a voltage can be driven by two perpendicular currents. It can survive under time-reversal symmetry and is sensitive to the breaking of discrete and crystal symmetries, which is unprecedented in the family of the Hall effects. The nonlinear Hall effect is quantum by nature because of its deep connection with the Berry curvature dipole. However, a full quantum description is still absent. Here we construct the quantum theory of the nonlinear Hall effect by using the diagrammatic techniques. We figure out totally 100 diagrams in 9 types that contribute to the leading nonlinear response in the weak-disorder limit. We show both qualitative and quantitative differences between the quantum theory and the semiclassical Boltzmann formulism. As an application of the diagrammatic results, we propose an experimental scheme to realize a pure electric detection of the Berry curvature distribution near the band edge. This work will be instructive for experimental and theoretical explorations of the topological physics beyond the linear regime.

Introduction.— The recent discovered nonlinear Hall effect [1–18] is a new member of the Hall family [19–22]. It is characterized as a nonlinear transverse voltage (or current) in response to two *ac* currents (or electric fields). The nonlinear Hall effect does not require broken time-reversal symmetry but inversion symmetry. More importantly, the nonlinear Hall effect is an unconventional response sensitive to the breaking of discrete and crystal symmetries, thus can be used to probe the spontaneous symmetry breaking transitions, such as nematic [23, 24], ferroelectric [25, 26] or even to a space symmetry related hidden order [27, 28]. More recently, it is proposed that the nonlinear Hall effect can also be used to probe the quantum critical point [3, 6, 15] and the Néel vector orientation in antiferromagnets [16]. Moreover, various related phenomena have also been proposed, such as the gyrotropic Hall [29], Magnus Hall [30] and nonlinear Nernst effect [31, 32].

The nonlinear Hall effect has a quantum nature because of its connection with the Berry curvature dipole. The Berry curvature can be regarded as a magnetic field in parameter space (e.g., momentum space). It describes the bending of the parameter space, arising from the geometrical structure of quantum eigen states. The Berry curvature dipole describes the dipole moment of the Berry curvature in momentum space [1]. However, by far all the works address the nonlinear Hall effect by using only the semiclassical Boltzmann formalism under the relaxation time approximation, such as band signatures [1, 6], disorder effects [9–11], high-frequency rectification [34], and gyrotropic Hall effects [29]. Moreover, the nonlinear Hall effect only appears in systems

without inversion symmetry, where the relaxation time approximation is not well applicable. There has been a tendency towards a quantum description of the nonlinear Hall effect [10, 11], and new side-jump contribution without semiclassical correspondence has also been discovered [10], but still relying on the semiclassical relaxation time approximation. A full quantum theory of the nonlinear Hall effect is still absent.

In this work, we construct a quantum theory for the nonlinear Hall effect using the diagrammatic techniques. Different from the bubble diagrams of the linear-response theory, the quadratic responses are depicted by triangular diagrams, representing two inputs and one output. We figure out totally 100 diagrams in 9 categories that contribute to the leading nonlinear responses for both time-reversal symmetric and broken systems in the weak-disorder limit, including the intrinsic, side-jump, skew-scattering, and trivial contributions (Fig. 1). We formulate the diagrams for a generic two-band model and apply them to calculate the nonlinear Hall conductivity of a disordered 2D tilted Dirac model. We find a step-like feature at the band edge, which is missing in the semiclassical Boltzmann formalism (Figs. 2 and 4). Based on the diagrammatic results, we propose an experimental scheme, which may realize a pure electric detection of the Berry curvature distribution near the band edge. The diagrammatic results can be generalized to first-principles calculations. Thus, the quantum theory will be instructive for both experimental and theoretical explorations of the topological physics beyond the linear regime.

Nonlinear response and triangular diagrams.— In response to *ac* electric fields along the *b* and *c* directions,

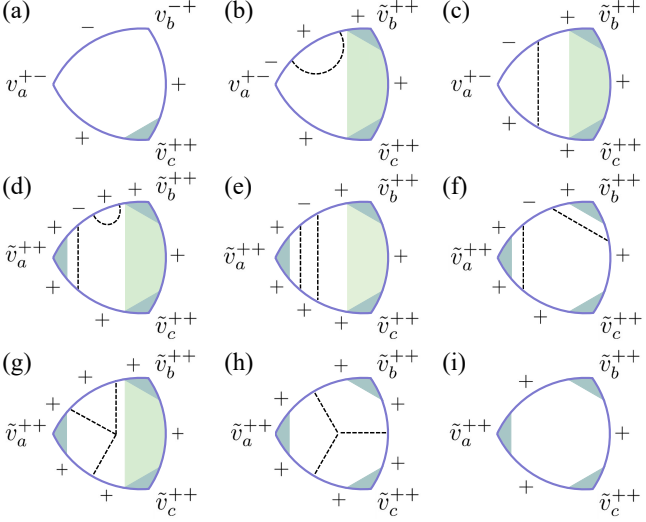


FIG. 1. The nonlinear Hall effect is characterized by a voltage (or current) induced by two perpendicular currents (or electric fields), so theoretically it can be depicted by the triangular diagrams with two inputs (v_b and v_c) and one output (v_a). The leading terms can be classified into the intrinsic (a), side-jump [(b)-(c)], intrinsic skew-scattering [(d)-(f)], extrinsic skew-scattering [(g)-(h)], and trivial (i) contributions. For (a)-(i), there are 6, 12, 24, 24, 12, 6, 12, 2, and 2 diagrams, respectively. The solid lines stand for the Matsubara Green's function of energy band + or - of a two-band model. The dash lines represent the disorder scattering. The dark and light shadows represent the vertex and edge disorder corrections, respectively. The edge corrections exist only in the nonlinear correlation functions [33].

the nonlinear electric current along the a direction can be formally written as [33]

$$\text{Re}[J_a^{(2)}(t)] = \bar{\xi}_{abc} \mathcal{E}_b \mathcal{E}_c \cos[(\omega_b - \omega_c)t] + \bar{\chi}_{abc} \mathcal{E}_b \mathcal{E}_c \cos[(\omega_b + \omega_c)t], \quad (1)$$

where $\{a, b, c\} \in \{x, y, z\}$, $\mathcal{E}_{b,c}$ and $\omega_{b,c}$ are the amplitudes and frequencies of electric fields, respectively. For a mono-frequency electric field input, $\bar{\xi}_{abc}$ and $\bar{\chi}_{abc}$ are the zero- and double-frequency responses, respectively, and $\bar{\xi}_{abc} = \bar{\chi}_{abc}$ by definition when $\omega_{b,c} = 0$. In experiments, it is more convenient to measure the double-frequency response, which is less sensitive to the low-frequency noise, so we focus on the diagrammatic calculation of $\bar{\chi}_{abc}$.

The quadratic nonlinear responses are depicted by the triangular diagrams (Fig. 1), i.e., two inputs and one output. In the weak-disorder limit, only the contributions in the leading order of the impurity concentration n_i are important, thus the corresponding diagrams can be selected according to their n_i dependence (see below). The representative diagrams for time reversal symmetric systems are shown in Fig. 1 (a)-(h), which can be further classified into intrinsic, side-jump, intrinsic and extrinsic skew-scattering contributions. While the diagrams for time reversal broken systems are shown in Fig. 1 (i).

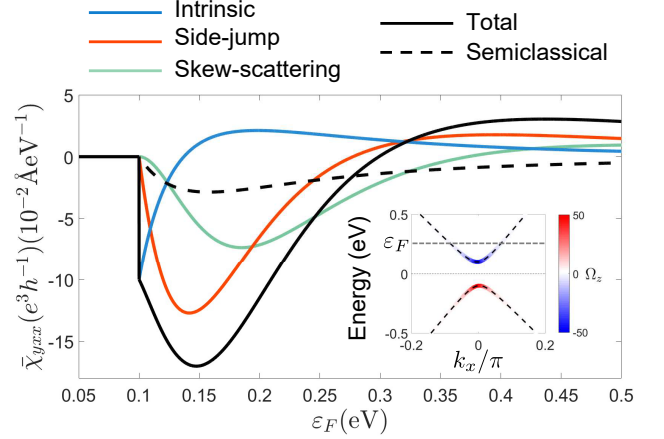


FIG. 2. Different contributions to the Nonlinear Hall conductivity $\bar{\chi}_{yxx}$ of the 2D tilted massive Dirac model [Eq. (4)] as functions of the Fermi energy ε_F at zero temperature. For comparison, the semiclassical result of the total contribution is also shown [9]. The newly defined $\bar{\chi}$ is different from χ [1, 6, 9] and $\bar{\chi}_{abc} \equiv 2\chi_{abc}$ in our specific case. The inset shows the two energy bands of the model. The color bar stands for the value of Berry curvature. The model parameters are $t = 0.1 \text{ eV} \cdot \text{\AA}$, $v = 1 \text{ eV} \cdot \text{\AA}$, $m = 0.1 \text{ eV}$, $n_i V_0^2 = 10^2 \text{ eV}^2 \cdot \text{\AA}^2$ and $n_i V_1^3 = 10^4 \text{ eV}^3 \cdot \text{\AA}^4$.

Generic model and disorder.— In order to construct the diagram techniques for disordered systems, we use a generic two-band model as a building block for realistic systems

$$\mathcal{H} = h_0 + h_x \sigma_x + h_y \sigma_y + h_z \sigma_z, \quad (2)$$

where $\sigma_{x,y,z}$ are the Pauli matrices, h_0 and $h_{x,y,z}$ are functions of the wave vector $\mathbf{k} = (k_x, k_y, k_z)$. The model describes two energy bands (denoted as \pm) with the band dispersions $\varepsilon_{\mathbf{k}}^{\pm} = h_0 \pm h_{\mathbf{k}}$, where $h_{\mathbf{k}} \equiv (h_x^2 + h_y^2 + h_z^2)^{1/2}$. The coupling to the electric field $E_a(t) = \mathcal{E}_a e^{-i\omega_a t}$ is considered as a perturbation [33] $\mathcal{H}' \approx -(ie/\omega_a)v_a E_a(t)$, where $-e$ is the electron charge and velocity operator $v_a \equiv \partial \mathcal{H} / \hbar \partial k_a$. Here we have neglected the multi-photon terms, which are important in quantum optics [35, 36] but less relevant in transport experiments. The disorder part is modeled as δ -function scatters $V_{imp}(\mathbf{r}) = \sum_i V_i \delta(\mathbf{r} - \mathbf{R}_i)$ with a random distribution \mathbf{R}_i and the disorder strength V_i satisfying $\langle V_i \rangle = 0$, $\langle V_i^2 \rangle = V_0^2$, and $\langle V_i^3 \rangle = V_1^3$, where $\langle \dots \rangle$ means the ensemble average over disorder configurations. Up to the leading order, the disorder scattering has two types of correlation, one correlates two scattering events [Fig. 1 (b)-(f)], and the other correlates three scattering events [Fig. 1 (g)-(h)].

The above considerations allow us to derive the expression of the nonlinear Hall conductivity for the generic two-band model [33]. The results are quite striking as we discover many new quantum contributions in the diagrammatic approach. For example, the intrinsic contribution for the + band in the zero-frequency limit is found

as [33]

$$\bar{\chi}_{abc}^{in} = -\frac{e^3}{2\hbar} \int [dk] \tau_k^+ \tilde{v}_{bk}^{++} \varepsilon^{acd} \Omega_{dk}^+ [f'(\varepsilon_k^+) + h_k f''(\varepsilon_k^+)] \\ + b \leftrightarrow c, \quad (3)$$

where $[dk] \equiv d^4\mathbf{k}/(2\pi)^4$, ζ stands for dimension, ε^{acd} is the Levi-Civita anti-symmetric tensor, τ_k^+ is the scattering time, \tilde{v}_{bk}^{++} is the vertex-corrected (by disorder) diagonal velocity, the Berry curvature [37] $\Omega_{ak}^i = -2\varepsilon^{abc}\hbar^2 \sum_{j \neq i} \text{Im}(v_{bk}^{ij} v_{ck}^{ji})/(\varepsilon_k^i - \varepsilon_k^j)^2$ with $i, j \in \pm$, $v_{ak}^{ij} \equiv \langle u_k^i | v_a | u_k^j \rangle$ and $|u_k^i\rangle$ are the eigen vectors of band i , $f = 1/\{1 + \exp[(\varepsilon_k^+ - \varepsilon_F)/k_B T]\}$ is the Fermi distribution with the Fermi energy ε_F , $f'(\varepsilon) \equiv \partial f(\varepsilon)/\partial \varepsilon$ and $f''(\varepsilon) \equiv \partial^2 f(\varepsilon)/\partial \varepsilon^2$. The f' term in Eq. (3) has been found as the Berry curvature dipole contribution [1, 2]. While the second f'' term is newly discovered, which was overlooked in the semiclassical formalism. The expressions of the side-jump and skew-scattering contributions can be found in [33], which also contain previously undiscovered terms.

Application to the 2D tilted Dirac model.— For an intuitive estimate of the quantum contributions, we apply the diagrams to calculate the nonlinear response for the 2D tilted Dirac model, whose Hamiltonian can be obtained by identifying

$$h_0 = tk_x, \quad h_x = vk_x, \quad h_y = vk_y, \quad h_z = m \quad (4)$$

in Eq. (2) with the model parameters t , v and m . This model is the minimal model of the nonlinear Hall effect because it has strong Berry curvature and no inversion symmetry [1, 6, 7]. t/v measures the tilt of the Dirac cone along the x direction, which breaks inversion symmetry. $2m$ is the band gap [6]. This model does not have time-reversal symmetry, and its time-reversal partner ($m \rightarrow -m$, $t \rightarrow -t$) at opposite regions of Brillouin zone [7] contribute the same nonlinear Hall response by symmetry with negligible coupling between the partners.

With the help of the diagrams, the nonlinear Hall conductivity $\bar{\chi}_{yxx}$ of the 2D Dirac model at zero temperature can be found [33], as shown in Fig. 2. The quantum result is about 5 or 6 times stronger than the semiclassical one due to the various newly found quantum contributions [33]. More strikingly, a step-like behavior appears in the quantum result, which is absent in the semiclassical theory, showing a qualitative difference. This step-like feature is solely contributed by the intrinsic mechanism, thus includes the information of the Berry curvature distribution. The side-jump and skew-scattering contributions obtained within the diagrammatic calculation are qualitatively consistent with those in the semiclassical formalism [9], but quantitatively enhanced, because of the finer treatment of the disorder scattering and new terms in the diagrammatic results [33]. However, no step-like behavior at the band edge are found for these extrinsic contributions, because of their strong dependence on the scattering processes.

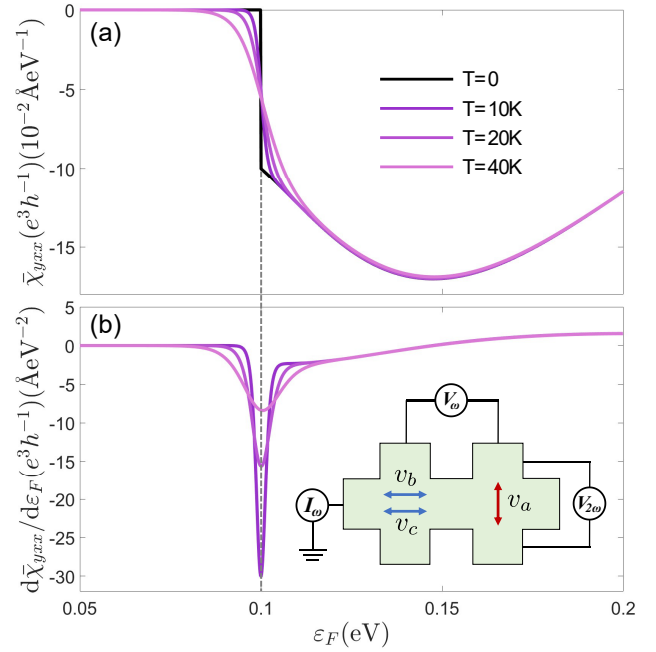


FIG. 3. (a) Total nonlinear Hall conductivity $\bar{\chi}_{yxx}$ of the 2D tilted massive Dirac model [Eq. (4)] versus the Fermi energy ε_F at different temperatures. (b) The derivative of (a) with respect to ε_F . Inset: The nonlinear Hall response can be measured in a standard Hall bar, by measuring the longitudinal single-frequency voltage V_ω and transverse double-frequency voltage $V_{2\omega}$ in response to a longitudinal ac current I_ω . The other parameters are the same as those in Fig. 2.

Experimental implications.— The Berry curvature dipole in the intrinsic contribution [Eq. (3)] opens a gate to explore higher-order topological responses. However, the intrinsic contribution is hard to measure because it is overwhelmed by the disorder contributions in most cases, according to the semiclassical results [9–11]. Nevertheless, according to our diagrammatic results, one can single out the Berry curvature dipole contribution by measuring the step-like feature in the nonlinear Hall response near the band edge [Fig. 3 (a)]. Specifically, one can measure the nonlinear Hall conductivity by scanning the Fermi energy at different temperatures. Because the step-like feature at the band edge is smoothed at finite temperatures, the peak in the derivative $d\bar{\chi}_{abc}/d\varepsilon_F$ [Fig. 3 (b)] can help us to identify the region of the step-like behaviour. By integrating the peak, one can extract the intrinsic contribution and the information of the Berry curvature dipole.

Figure 3 demonstrates a specific case to measure $\bar{\chi}_{yxx}$. The driving current I_ω oscillating at ω is applied along the x direction. The single- and double-frequency voltages V_ω and $V_{2\omega}$ are measured along the x and y directions, respectively. $\bar{\chi}_{yxx}$ can be found as [6, 8, 9]

$$\bar{\chi}_{yxx} = V_{2\omega} I_\omega / (V_\omega)^3. \quad (5)$$

The Fermi energy can be scanned by tuning the gate volt-

ages in 2D devices [7]. Moreover, the dominance of the intrinsic contribution near the band edge can be verified experimentally by fixing the Fermi energy near the band edge and performing the scaling experiments, similar to those in [9].

Analysis of the band-edge behavior.— The qualitative difference between the quantum and semiclassical results mainly lies at the band edge [Fig. 2], which is solely contributed by the intrinsic mechanism. We find that this step-like band-edge behavior in 2D is a consequence of the f'' term in Eq. (3). As both $f'(\varepsilon_k^+)$ and $h_k f''(\varepsilon_k^+)$ transform like scalar (specifically ε_k^\pm) under symmetry operations, the f'' term shares the same symmetry with the Berry curvature dipole [1]. However, this contribution was overlooked in the semiclassical formalism. In the semiclassical formalism, the electric field \mathcal{E} drives the current by inducing a variation of the distribution $\delta f \sim \mathcal{E} f' + \mathcal{E}^2 f'' + \dots$ [1, 6, 9, 10, 29, 34]. Meanwhile, the Berry curvature Ω comes in the current also with an electric field [37]. Consequently, the $f''\Omega$ term is of order \mathcal{E}^3 thus dropped in the \mathcal{E}^2 response. By contrast, in the quantum theory, the Fermi distribution f does not depend on \mathcal{E} [38] and the resultant f'' term is of order \mathcal{E}^2 , thus should be allowed in Eq. (3).

Figure 4 (a) demonstrates the nonlinear Hall conductivity contributed by the f' and f'' terms. The contribution from f' term vanishes at the band edge while that from f'' term remains finite. This behaviour can be understood by writing the f'' term as a Fermi surface integral (Note that $f' \approx \delta(\varepsilon - \varepsilon_F)$ at low temperatures) using integration by parts

$$\bar{\chi}_{abc}^{in(2)} = \frac{e^3}{2\hbar} \int [dk] \varepsilon^{acd} \frac{\partial(\eta_v \tau_k^+ \Omega_{dk}^+ h_k)}{\partial k_b} f'(\varepsilon_k^+) + b \leftrightarrow c, \quad (6)$$

where $\eta_v \equiv \tilde{v}_{bk}^{++}/v_{bk}^{++} \in [1, 2]$ is the velocity correction from the ladder diagram. The f'' term becomes a Fermi surface integration of the quantity proportional to $\partial(\Omega_{dk}^+ h_k)/\partial k_b$, which governs the band edge behaviour. As the band edge is defined by equations $\partial(\varepsilon_k^+)/\partial k_a = 0$, where the band velocity vanishes. Thus the Fermi surface integration of $-\Omega_{dk}^+ v_{bk}^{++}$ (the f' term) always vanishes at the band edge, as the integrand equals to zero at the band bottom [Figs. 4 (b)]. On the other hand, as we have $\partial(\Omega_{dk}^+ h_k)/\partial k_b \sim \Omega_{dk}^+(v_{bk}^{++} - v_{bk}^{--})$, the integrand of f'' term does not vanish because the band edge of the upper and lower bands are not located at the same k point for tilted band systems [Figs. 4 (b)]. Moreover, the contribution from the f'' term increases as the band tilt grows, thus the step-like behaviour at the band edge can be enhanced in systems close to Lifshitz transition [6].

Diagrammatic analysis.— Last but not the least, we discuss the implications of the diagrams. In the weak-disorder limit, the diagrams of leading contribution are constructed according to their dependence on the impurity concentration n_i . The strongest nonlinear transport

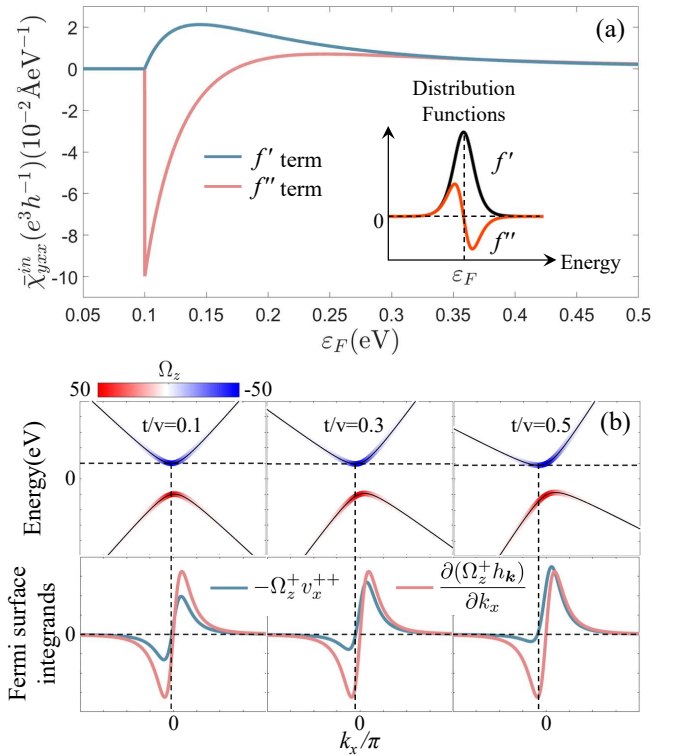


FIG. 4. (a) The nonlinear Hall conductivity contributed by the f' and f'' terms at zero temperature. Inset: f'' is the second derivative of the Fermi distribution and is opposite at opposite wave vectors. (b) The simplified Fermi surface integrands of f' and f'' terms in systems with different tilting parameters t/v . Here $k_y = 0$ and the other parameters are the same as those in Fig. 2.

contribution a triangular diagram can support is of order n_i^{-2} . In the chiral basis, there is only one type of these diagrams [Fig. 1 (i)], which we referred to as trivial because their contribution

$$\bar{\chi}_{abc}^{tr} = -\frac{e^3}{2} \int [dk] (\tau_k^+)^2 \tilde{v}_{ak}^{++} \tilde{v}_{bk}^{++} v_{ck}^{++} f''(\varepsilon_k^+) + b \leftrightarrow c \quad (7)$$

is irrelevant with any geometrical property of the system. This term governs both the transverse and longitudinal quadratic nonlinear transports in the weak-disorder limit if not vanishes. However, according to the general expression, this contribution only exists in time-reversal broken systems.

For systems with time-reversal symmetry, the leading contribution to the nonlinear transport is of order n_i^{-1} , which can be obtained by adding non ladder type scattering events on the trivial diagrams. The resultant diagrams of order n_i^{-1} within the non-crossed approximation are shown in Fig. 1 (a)-(h), which include intrinsic, side-jump, intrinsic and extrinsic skew-scattering contributions. For the intrinsic contribution [Fig. 1 (a)], there are totally 6 diagrams, which can be identified by noting that [33] $(\varepsilon^{abc}/h^2)\Omega_{ck}^\pm = \mp \text{Im}(v_{ak}^{+-} v_{bk}^{-+})/2h_k^2$. And

the resultant expression for a general two-band model is Eq. (3).

For the side-jump contribution [Figs. 1 (b)-(c)], there are totally 36 diagrams in 2 categories. They can be identified by the characteristic quantity $v_{ak}^{+-}\langle V_{kk'}^{-+}V_{k'k}^{++}\rangle$ with $V_{kk'}^{-+} \equiv \langle u_{\mathbf{k}}^- | V_{imp} | u_{\mathbf{k}'}^+ \rangle$. This quantity represents an off-diagonal scattering process, which is connected to the side-jump velocity via

$$v_{ak}^{sj} = \pi \int [dk'] \delta(\varepsilon_{\mathbf{k}}^+ - \varepsilon_{\mathbf{k}'}^+) \times \text{Im} \left[\frac{v_{ak}^{+-}\langle V_{kk'}^{-+}V_{k'k}^{++}\rangle}{h_{\mathbf{k}}} - \frac{v_{ak'}^{+-}\langle V_{k'k}^{-+}V_{kk'}^{++}\rangle}{h_{\mathbf{k}'}} \right]. \quad (8)$$

Different from the linear side-jump contribution which is only relevant to the side-jump velocity [21, 39, 40], the nonlinear side-jump contribution has three types of similar quantities [33]. According to their physical mechanisms, these 36 diagrams can be classified into two categories. The first one is due to the accumulation of the coordinate shifts after many scatterings, thus corresponds to the diagrams with off-diagonal velocity elements in the output vertex (v_a in Fig. 1). The second one is due to the anomalous correction to the distribution function, thus corresponds to the diagrams with diagonal output vertex, that is, all the off-diagonal velocity elements appear in the input vertex (v_b or v_c in Fig. 1). The triangular diagram has a three-fold rotation symmetry, so the first category has 12 diagrams while the second one contains 24 diagrams [33].

The skew-scattering contribution contains the diagrams with only diagonal velocity elements, which can be classified into two categories as intrinsic [Fig. 1 (d)-(f)] and extrinsic [Fig. 1 (g)-(h)] skew-scattering according to their characteristic scattering processes [33]. The first one is from the leading asymmetric scattering contribution due to the Gaussian disorder within the non-crossing approximation, and is featured by the scattering processes $\langle V_{kk'}^{-+}V_{k'k}^{++}\rangle\langle V_{k''k}^{+-}V_{kk''}^{++}\rangle$ with totally 42 diagrams in 3 categories. The second one is from the leading asymmetric scattering contribution due to the non-Gaussian disorder, and is featured by the scattering processes $\langle V_{kk'}^{++}V_{k'k''}^{++}V_{k''k}^{++}\rangle$ with totally 14 diagrams in 2 categories.

We thank helpful discussions with Huimei Liu and Suyang Xu. This work was supported by the Strategic Priority Research Program of Chinese Academy of Sciences (XDB28000000), the National Basic Research Program of China (2015CB921102), the National Key R&D Program (2016YFA0301700), the Guangdong Innovative and Entrepreneurial Research Team Program (2016ZT06D348), the National Natural Science Foundation of China (11534001, 11974249, 11925402, 11404106), the Natural Science Foundation of Shanghai (19ZR1437300), and the Science, Technology and Innovation Commission of Shenzhen Municipality (ZDSYS20170303165926217, KYT-

DPT20181011104202253, G02206304, and G02206404). The numerical calculations were supported by Center for Computational Science and Engineering of Southern University of Science and Technology.

* Corresponding author: luhz@sustech.edu.cn

- [1] I. Sodemann and L. Fu, “Quantum nonlinear Hall effect induced by berry curvature dipole in time-reversal invariant materials”, *Phys. Rev. Lett.* **115**, 216806 (2015).
- [2] T. Low, Y. Jiang, and F. Guinea, “Topological currents in black phosphorus with broken inversion symmetry”, *Phys. Rev. B* **92**, 235447 (2015).
- [3] J. I. Facio, D. Efremov, K. Koepernik, J.-S. You, I. Sodemann, and J. van den Brink, “Strongly enhanced Berry dipole at topological phase transitions in BiTeI”, *Phys. Rev. Lett.* **121**, 246403 (2018).
- [4] J.-S. You, S. Fang, S.-Y. Xu, E. Kaxiras, and T. Low, “Berry curvature dipole current in the transition metal dichalcogenides family”, *Phys. Rev. B* **98**, 121109(R) (2018).
- [5] Y. Zhang, J. van den Brink, C. Felser, and B. Yan, “Electrically tuneable nonlinear anomalous Hall effect in two-dimensional transition-metal dichalcogenides WTe₂ and MoTe₂”, *2D Materials* **5**, 044001 (2018).
- [6] Z. Z. Du, C. M. Wang, H.-Z. Lu, and X. C. Xie, “Band signatures for strong nonlinear Hall effect in bilayer WTe₂”, *Phys. Rev. Lett.* **121**, 266601 (2018).
- [7] Q. Ma, S.-Y. Xu, H. Shen, D. MacNeill, V. Fatemi, T.-R. Chang, *et al.*, “Observation of the nonlinear Hall effect under time-reversal-symmetric conditions”, *Nature* **565**, 337 (2019).
- [8] K. Kang, T. Li, E. Sohn, J. Shan, and K. F. Mak, “Observation of the nonlinear anomalous Hall effect in 2D WTe₂”, *Nature Mater.* **18**, 324 (2019).
- [9] Z. Z. Du, C. M. Wang, S. Li, H.-Z. Lu, and X. C. Xie, “Disorder-induced nonlinear Hall effect with time-reversal symmetry”, *Nature Commun.* **10**, 3047 (2019).
- [10] C. Xiao, Z. Z. Du, and Q. Niu, “Theory of nonlinear Hall effects: Modified semiclassics from quantum kinetics”, *Phys. Rev. B* **100**, 165422 (2019).
- [11] S. Nandy and I. Sodemann, “Symmetry and quantum kinetics of the nonlinear Hall effect”, *Phys. Rev. B* **100**, 195117 (2019).
- [12] O. Matsyshyn and I. Sodemann, “Nonlinear Hall acceleration and the quantum rectification sum rule”, *Phys. Rev. Lett.* **123**, 246602 (2019).
- [13] H. Wang and X. Qian, “Ferroelectric nonlinear anomalous Hall effect in few-layer WTe₂”, *npj Comput. Mater.* **5**, 1 (2019).
- [14] B. T. Zhou, C.-P. Zhang, and K. T. Law, “Highly tunable nonlinear Hall effects induced by spin-orbit couplings in strained polar transition-metal dichalcogenides”, *Phys. Rev. Applied* **13**, 024053 (2020).
- [15] H. Rostami and V. Jurićć, “Probing quantum criticality using nonlinear Hall effect in a metallic dirac system”, *Phys. Rev. Research* **2**, 013069 (2020).
- [16] D.-F. Shao, S.-H. Zhang, G. Gurung, W. Yang, and E. Y. Tsymbal, “Nonlinear anomalous Hall effect for Néel vector detection”, *Phys. Rev. Lett.* **124**, 067203 (2020).
- [17] S. Singh, J. Kim, K. M. Rabe, and D. Vanderbilt, “En-

gineering Weyl phases and nonlinear Hall effects in T_d - MoTe_2 ”, [arXiv:2001.08283](https://arxiv.org/abs/2001.08283) (2020).

[18] M. W.-Y. Tu, C. Li, H. Yu, and W. Yao, “Non-adiabatic Hall effect at Berry curvature hot spot”, [arXiv:2004.01326](https://arxiv.org/abs/2004.01326) (2020).

[19] K. v. Klitzing, G. Dorda, and M. Pepper, “New method for high-accuracy determination of the fine-structure constant based on quantized Hall resistance”, *Phys. Rev. Lett.* **45**, 494 (1980).

[20] M. E. Cage, K. Klitzing, A. Chang, F. Duncan, M. Haldane, R. Laughlin, A. Pruisken, D. Thouless, R. E. Prange, and S. M. Girvin, *The quantum Hall effect* (Springer Science & Business Media, 2012).

[21] N. Nagaosa, J. Sinova, S. Onoda, A. H. MacDonald, and N. P. Ong, “Anomalous Hall effect”, *Rev. Mod. Phys.* **82**, 1539 (2010).

[22] K. Yasuda, R. Wakatsuki, T. Morimoto, R. Yoshimi, A. Tsukazaki, K. S. Takahashi, M. Ezawa, M. Kawasaki, N. Nagaosa, and Y. Tokura, “Geometric Hall effects in topological insulator heterostructures”, *Nature Phys.* **12**, 555 (2016).

[23] S. Saha and G. K. Wong, “Investigation of nematic ordering using electric-field-induced second-harmonic generation”, *Applied Physics Letters* **34**, 423 (1979).

[24] W. Chen, M. B. Feller, and Y. R. Shen, “Investigation of anisotropic molecular orientational distributions of liquid-crystal monolayers by optical second-harmonic generation”, *Phys. Rev. Lett.* **63**, 2665 (1989).

[25] A. M. Pugachev, V. I. Kovalevskii, N. V. Surovtsev, S. Kojima, S. A. Prosandeev, I. P. Raevski, and S. I. Raevskaya, “Broken local symmetry in paraelectric BaTiO_3 proved by second harmonic generation”, *Phys. Rev. Lett.* **108**, 247601 (2012).

[26] R.-C. Xiao, D.-F. Shao, W. Huang, and H. Jiang, “Electrical detection of ferroelectric-like metals through nonlinear Hall effect”, [arXiv:2004.06913](https://arxiv.org/abs/2004.06913) (2020).

[27] L. Zhao, D. Torchinsky, H. Chu, V. Ivanov, R. Lifshitz, R. Flint, T. Qi, G. Cao, and D. Hsieh, “Evidence of an odd-parity hidden order in a spin-orbit coupled correlated iridate”, *Nature Physics* **12**, 32 (2016).

[28] L. Zhao, C. Belvin, R. Liang, D. Bonn, W. Hardy, N. Armitage, and D. Hsieh, “A global inversion-symmetry-broken phase inside the pseudogap region of $\text{YBa}_2\text{Cu}_3\text{O}_y$ ”, *Nature Physics* **13**, 250 (2017).

[29] E. J. König, M. Dzero, A. Levchenko, and D. A. Pesin, “Gyrotropic Hall effect in Berry-curved materials”, *Phys. Rev. B* **99**, 155404 (2019).

[30] M. Papaj and L. Fu, “Magnus Hall effect”, *Phys. Rev. Lett.* **123**, 216802 (2019).

[31] X.-Q. Yu, Z.-G. Zhu, J.-S. You, T. Low, and G. Su, “Topological nonlinear anomalous Nernst effect in strained transition metal dichalcogenides”, *Phys. Rev. B* **99**, 201410(R) (2019).

[32] C. Zeng, S. Nandy, A. Taraphder, and S. Tewari, “Nonlinear Nernst effect in bilayer WTe_2 ”, *Phys. Rev. B* **100**, 245102 (2019).

[33] Supplemental Material.

[34] H. Isobe, S.-Y. Xu, and L. Fu, “High-frequency rectification via chiral Bloch electrons”, *Sci. Adv.* **6**, eaay2497 (2020).

[35] D. E. Parker, T. Morimoto, J. Orenstein, and J. E. Moore, “Diagrammatic approach to nonlinear optical response with application to Weyl semimetals”, *Phys. Rev. B* **99**, 045121 (2019).

[36] Z. Li, T. Tohyama, T. Iitaka, H. Su, and H. Zeng, “Nonlinear optical response from quantum kinetic equation”, [arXiv:2001.07839](https://arxiv.org/abs/2001.07839) (2020).

[37] D. Xiao, M. C. Chang, and Q. Niu, “Berry phase effects on electronic properties”, *Rev. Mod. Phys.* **82**, 1959 (2010).

[38] G. D. Mahan, *Many-Particle Physics* (Plenum Press, 1990).

[39] N. A. Siniatsyn, “Semiclassical theories of the anomalous Hall effect”, *J. Phys.: Condens. Matter* **20**, 023201 (2008).

[40] N. A. Siniatsyn, A. H. MacDonald, T. Jungwirth, V. K. Dugaev, and J. Sinova, “Anomalous Hall effect in a two-dimensional Dirac band: The link between the Kubo-Streda formula and the semiclassical Boltzmann equation approach”, *Phys. Rev. B* **75**, 045315 (2007).